FINITE ELEMENTS SIMULATION OF A CASE HARDENING PROCESS

Dan Birsan[1]

[1] *"Dunarea de Jos" University of Galati, dbirsan@ugal.ro.*

Abstract: *This paper presents a detailed simulation study of a case hardening process using Simufact Forming software. The simulation captures various stages of case hardening including heating to carburizing temperature, carburizing, diffusion to equalize the carbon profile, quenching, and cooling to room temperature. The primary focus is on modeling the thermal and diffusion behaviors to examine microstructural changes in the material, utilizing finite element analysis to predict and visualize the distribution of carbon concentration and the formation of martensite during quenching. The workpiece material used in the simulation is S690QL steel, and the results are validated against theoretical predictions and empirical data. The simulation outcomes offer insights into optimizing the heat treatment process parameters to enhance material properties, demonstrating the potential of integrating multiple processing technologies on a single machine tool base for improved efficiency and effectiveness in industrial applications. This study is significant for engineers and researchers involved in materials science and manufacturing processes, providing a robust framework for understanding and improving case hardening techniques.*

Keywords: *hardening, diffusion, carburizing, finite element*

1. Introduction

This document outlines the simulation of a case hardening process using Simufact Forming software, focusing on the necessary steps and configurations for modeling and simulation in the context of heat treatment and phase transformation effects. The case hardening process simulation involves several stages: heating the workpiece to the carburizing temperature, carburizing, diffusion to equalize the carbon profile, cooling down to hardening temperature, quenching in oil, and finally cooling down to room temperature. The simulation models thermal and diffusion behaviors to understand the microstructural changes in the material.

The setup involves configuring the simulation environment in Simufact.Forming, selecting appropriate material data sets, and defining the geometrical and process parameters such as temperature, time, and carbon potential. The software enables the adjustment of parameters to reflect various industrial scenarios, providing flexibility in modeling different case hardening conditions.

The study presents by Maximov et al. Ref. [1] assesses the effectiveness of roller burnishing (RB) and slide roller burnishing (SRB) on AISI 316 steel's surface integrity, highlighting improvements in microhardness and roughness parameters. It introduces a novel slide roller burnishing method, using a toroidal roller that crosses the workpiece axis, resulting in enhanced surface properties through effective strain hardening and reduced surface roughness. Comparative analyses between RB and SRB reveal that SRB achieves superior surface finishing by optimizing the crossing angle and burnishing parameters, making it advantageous for industrial applications requiring high surface integrity.

Jászfi et al. Ref. [2] presents a study that explores the efficiency of surface-thermal hardening of machine parts under the integration of multiple processing technologies on a single machine tool base. It examines the

interplay between various hardening processes and the resultant material properties, highlighting improvements in process efficiency and effectiveness. The findings suggest that integrating multiple technologies not only optimizes the hardening process but also enhances the mechanical properties of the machine parts.

Holmberg et al. Ref. [3] presents a study that examines the progressive induction hardening process, focusing on the measurement and alteration of residual stresses in C45E steel. The research highlights the impact of different scanning speeds on residual stress distribution, where faster scanning leads to higher tensile residual stresses in the transition zone. The study uses x-ray diffraction and layer removal methods to quantify these stresses, providing insights into optimizing the induction hardening process for enhanced fatigue performance. Findings suggest that controlling the energy input and scanning speed can significantly influence the residual stress profiles, particularly in critical areas prone to fatigue.

The document presented by Smirnov et al. Ref. [4] represents a study on improving the efficiency of surface-thermal hardening of machine parts by integrating multiple processing technologies on a single machine tool base. It details the process enhancements that contribute to more durable and precise machine parts. The study demonstrates how combining advanced thermal treatments with precision machining can significantly enhance production efficiency and part performance.

Pinheiro et al. Ref [5] presents the optimization of the induction hardening process for gears, focusing on minimizing distortions and enhancing material properties. The methodology includes detailed simulations of thermal and structural behavior using the Ansys platform, validated by experimental data. Key findings suggest improvements in the precision and cost-effectiveness of gear manufacturing, with proposed strategies for reducing energy consumption and enhancing overall component performance.

Spezzapria et al. Ref. [6] presents a multi-scale multiphysical finite element analysis for predicting microstructural evolution during induction hardening, focusing on phase transformations in steel components. An ad hoc code calculates metallurgical phase changes during the heating and cooling phases, coupled with FEM software to handle the electromagnetic and thermal problems. Results highlight the accuracy of the model in predicting temperature distribution and phase transformations, offering a robust tool for enhancing the quality and efficiency of induction hardening processes.

The paper by Javaheri et al. Ref. [7] presents an induction hardening of a new medium-carbon, low-alloy wear resistance steel, utilizing Flux2D software and a Gleeble thermomechanical simulator to predict material property profiles. The study focuses on optimizing induction hardening parameters to achieve desired microstructure and hardness profiles through the thickness of slurry transportation pipes. Results confirm the effectiveness of coupling phase transformation modeling with thermal cycle predictions to tailor material properties for specific applications.

2. Numerical Model

The application module Heat treatment of Simufact Forming software use a dedicated process type "Case hardening" for the simulation of the process. This process type uses a typical sequence of a direct hardening process:

- Heating (to carburizing temperature);
- Carburizing;
- Diffusion (to equalize the carbon profile);
- Cool down (to hardening temperature);
- Quenching;
- Cooling (to room temperature).

In Fig. 1 can be seen the finite element model used which consists of a discretized part with 2D elements designed for the analysis of 2D axiometric problems, known as Quad (10) in Simufact Forming terminology Ref. [10].

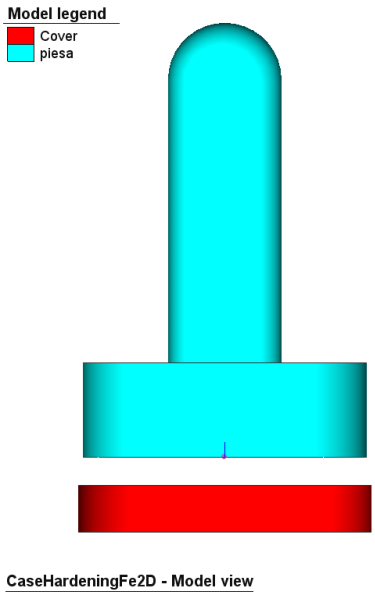

Figure 1: *3D finite elements model*

The workpiece material used S690QL steel has been used in this simulation and Table 1 shows the chemical composition.

Table 1: *S690QL chemical composition (%)*

Element	Min	Max	Fix
C	0	0	0.16
Cr	0	0	0.55
Fe	0	0	96.963
Mn	0	0	1.45
Mo	0	0	0.37
Ni	0	0	0.15
P	0	0	0.012
S	0	0	0.005
Si	0	0	0.3
V	0	0	0.04

Mechanical properties

- Young's modulus:

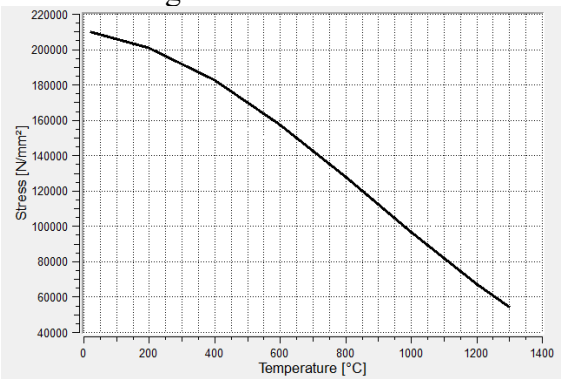

Figure 2: *Young's modulus versus temperature*

- Poisson's ratio:

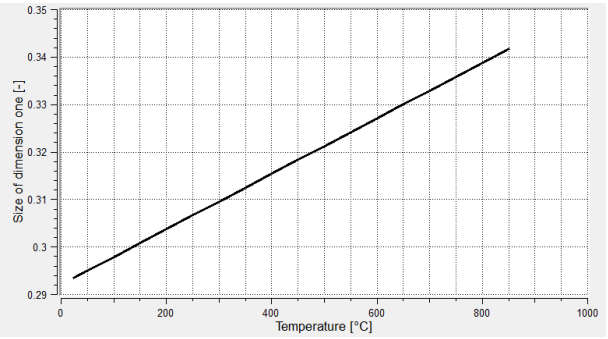

Figure 3: *Poisson's ratio versus temperature*

- Density:

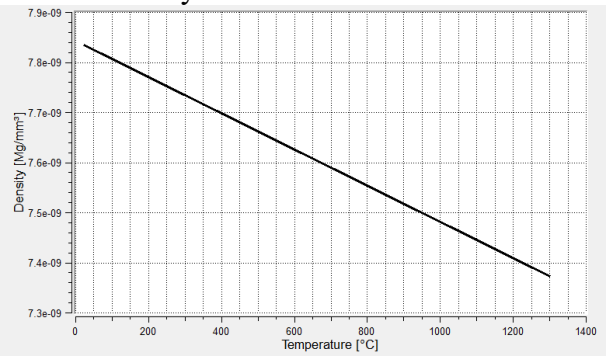

Figure 4: *Density versus temperature*

Thermal properties

- Thermal conductivity:

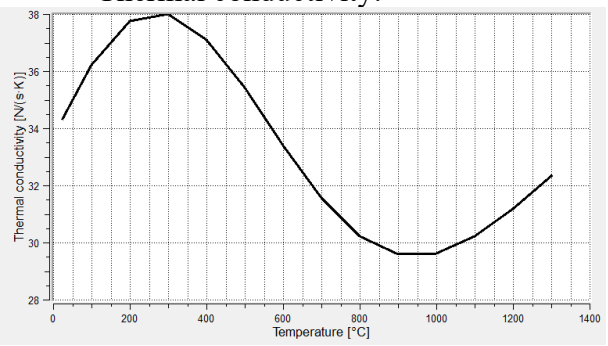

Figure 5: *Thermal conductivity versus temperature*

- Specific heat capacity:

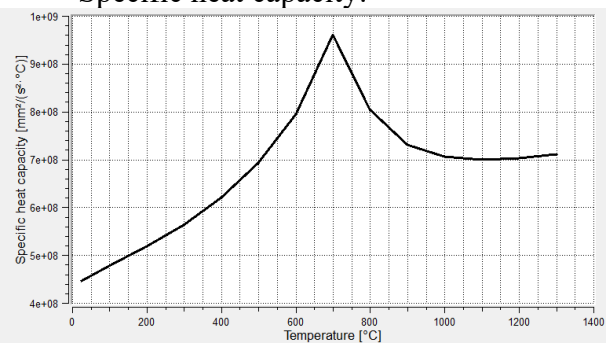

Figure 6: *Specific heat capacity versus temperature*

- Melting temperature: 1509.95 °C;
- Solidus temperature: 1462.92 °C;
- Latent heat for melting: 256400.0 J/kg;
- Dissipation factor: 0.9.

Fig.7 shows the material flow stress obtained from the material database integrated into the Simufact Forming software Ref. [10]. They correspond to a temperature and strain rate-dependent material model based on the MatiLDa database.

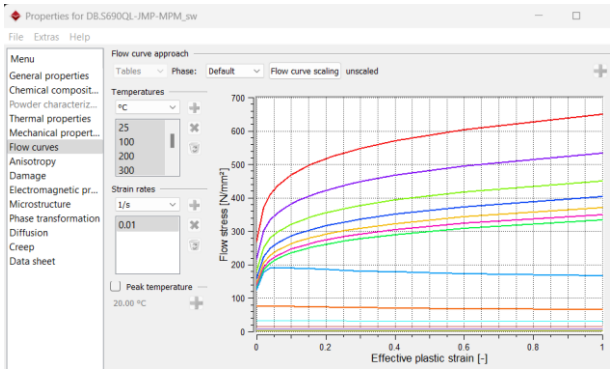

Figure 7: *Flow stress versus temperature*

Phase transformation

- CCT

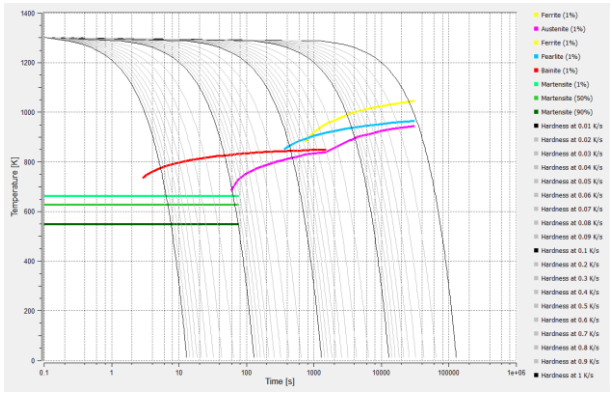

Figure 8: *CCT diagram*

- TTT

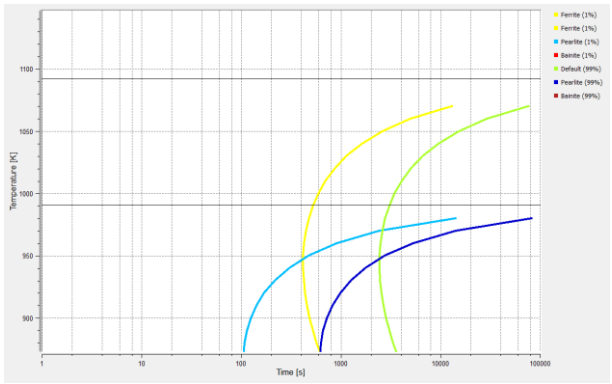

Figure 9: *TTT diagram*

For simulating case hardening processes, the implementation of a diffusion pass has been considered in the solver. The heat equation and the diffusion equation are mathematically identical, differing only in the numerical values of their parameters. This equivalence simplifies the modelling of thermal and diffusion phenomena, suggesting that tools and methods developed for thermal analysis can be adapted for diffusion analysis.

$$\frac{\partial Q}{\partial t} + \nabla F = 0 \qquad (1)$$

where Q is the variable and $F = F_{convection} + F_{diffusion}$ is the corresponding flux, consisting of convection and diffusion terms.

The solver includes a diffusion pass designed specifically to solve the diffusion equation. This feature enables the simulation of the diffusion of elements, such as carbon, into materials like Austenite, which is essential for case hardening.

The following settings were used for the direct hardening process:

- 11 min heating the workpiece to the carburizing temperature of 900 °C;
- 40 min carburizing at 900°C with a carbon potential of 1.1 %;
- 20 min diffusion at 900°C with 0,75 % carbon potential;
- 12 min reducing the furnace temperature from 900 °C to annealing temperature of 850 °C;
- 1 min quenching the part in oil at 70 °C;
- 6 min final cooling to room temperature in still air.

For later investigation of the carbon profile the post particles were added in the model (see Fig. 10).

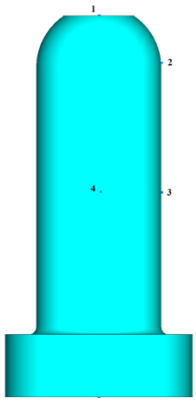

Figure 10: *The points particles to the workpiece*

3. Results

The analysis begins with an overview of the carbon concentration at the conclusion of the carburization and diffusion steps, Figs. 11, 12. It is observed that the local carbon concentration remained at the base material level due to the coating on the underside of the part. In addition, it is observed that the local carbon concentration in the carburized layer is significantly affected by the actual shape of the workpiece.

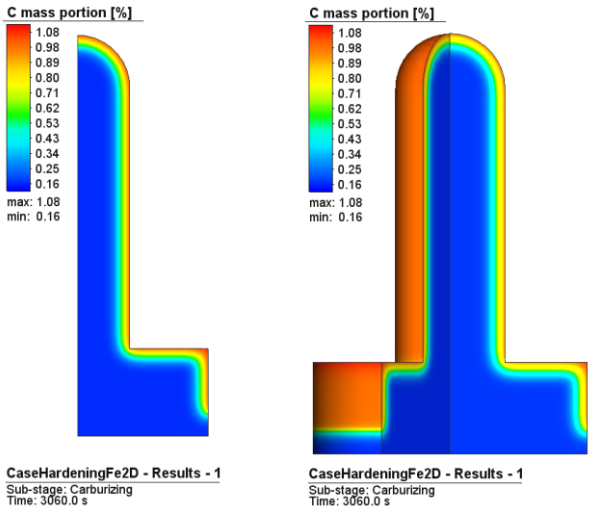

Figure 11: *Carbon distribution at the end of stages Carburizing*

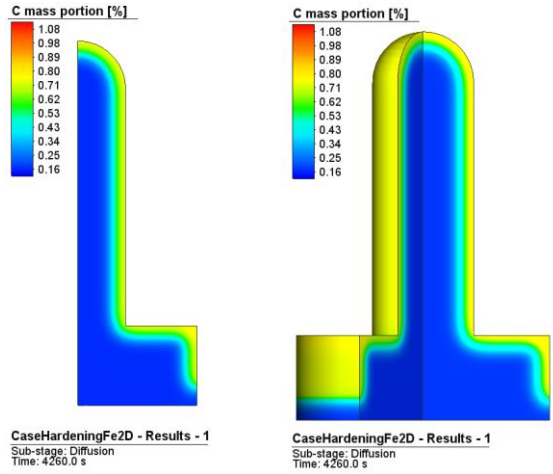

Figure 12: *Carbon distribution at the end of stages Diffusion*

In Fig. 13 simulation results can be seen for the martensite volume fraction of a workpiece during the quenching phase of the heat treatment process.

In the first image it can see the early stage of quenching. The color scale, ranging from blue to red (0 to 100%), indicates the volume fraction of martensite formed. The blue areas suggest little to no martensite, typically representing regions that are cooler or have slower cooling rates. The green areas indicate a transition, showing an intermediate amount of martensite formation.

In this middle stage, we see a significant increase in the formation of martensite, as indicated by the expansion of green, yellow, and orange areas. This suggests higher temperatures or regions experiencing faster cooling rates conducive to martensite formation. The clear gradient from the outer edges toward the center indicates how the quenching medium's effectiveness and heat transfer rates impact martensite formation.

The final view shows nearly complete transformation in many parts of the workpiece, with most areas in orange and red, indicating a high-volume fraction of martensite. This stage represents a more advanced quenching process where the majority of the material has transformed, likely achieving the desired hardness and material properties.

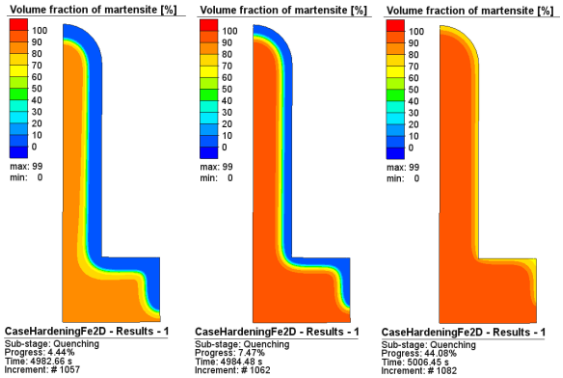

Figure 13: *Martensite evolution during Quenching*

Each stage represents a snapshot in time during the quenching process, illustrating how different regions of the workpiece cool and transform at different rates based on their exposure to the cooling medium, geometry, and material properties. These

results are crucial for understanding the effectiveness of the heat treatment process and predicting the final properties of the treated material.

In order to investigate the evolution of the local carbon concentration, graphs were plotted, Fig. 14, for the particles that were defined before the simulation started (see Fig. 10).

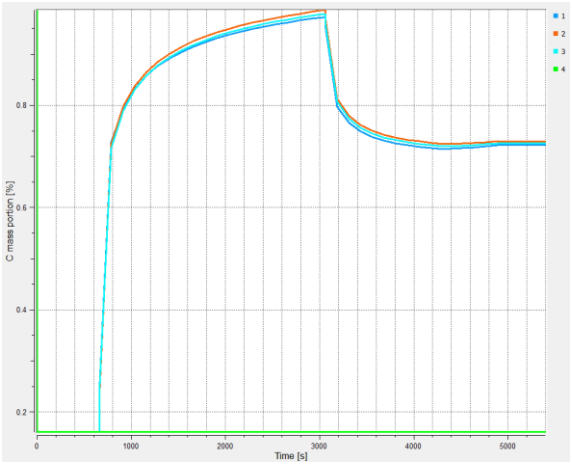

Figure 14: *Evolution of surface carbon concentration on surface particle*

Initial phase (0 to 660 seconds):

The graph starts with a very low carbon mass fraction close to zero, indicating that no significant carbon diffusion or increase is occurring in the early stage of the process.

This flat line suggests that the material is not yet undergoing carburizing, or that the process parameters are not yet conducive to carbon diffusion.

Rapid carbon increase (660 to 1600 s):

Around the 660-second mark, there is a sharp and rapid increase in the carbon mass fraction. This abrupt rise means that the carburizing process has been initiated or that conditions for carbon absorption in the material have changed suddenly. It indicates the start of diffusion when the material reaches an appropriate temperature or atmosphere composition for carbon diffusion to occur.

Plateau (1600 to 3060 s):

After the sharp increase, the carbon mass fraction reaches a maximum level, stabilizing at around 0.85%. This plateau means that the carburizing process has achieved a steady-state condition where the carbon concentration in the surface region has reached its desired level, or the saturation point for carbon diffusion has been reached.

Drop in carbon fraction (3060 to 4260 s):

A significant drop in carbon mass fraction occurs after the peak, indicating a change in conditions, such as the start of a diffusion phase. This represents the redistribution of carbon deeper into the material or the loss of carbon from the surface due to a change in process parameters.

Final Stabilization (4260 s onward):

After the drop, the carbon mass fraction levels out again, remaining relatively constant. This suggests that the material has reached a new equilibrium state where carbon diffusion has stopped. This phase represents the end of the carburizing process.

This graph illustrates a typical carburizing process where carbon is diffused into the material, with a rapid increase in carbon content, followed by redistribution or a drop, due to the cooling phase.

The sharp increase indicates that the process of carburizing is highly time-sensitive and dependent on specific conditions being met, while the drop and stabilization suggest redistribution has a notable effect on the carbon concentration. This graph can be useful for understanding the kinetics of carbon absorption and diffusion during heat treatment processes.

The combined image Fig. 15 showcases in two different visualizations related to carbon distribution in a material undergoing a carburizing process. The graph on the right depicts the carbon mass fraction along the distance from the surface into the depth of the material. It starts from a high concentration at the surface (matching the high values shown in the thermal image) and sharply declines as it moves deeper into the material. This corresponds with the

visual color gradient on the left side, demonstrating how the carbon concentration decreases from the treated surface inward. These visualizations are essential for understanding how carbon is distributed within the material after carburizing, providing insights into the effectiveness of the heat treatment and its impact on material properties such as wear resistance and hardness. The steep gradient in the graph and the corresponding high carbon concentration at the surface visible in the simulation are indicators of a successful surface hardening process.

The combined image Fig. 16 depicts a carbon concentration profile across a material, showing a steep decline in carbon mass proportion from nearly 1% to about 0.1% over a distance of 1.5 millimeters, indicative of a gradient created perhaps by a diffusion process.

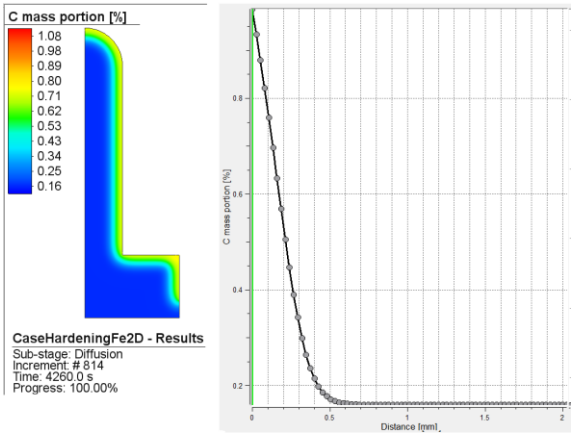

Figure 15: *Carbon profile at the end of stage Carburizing*

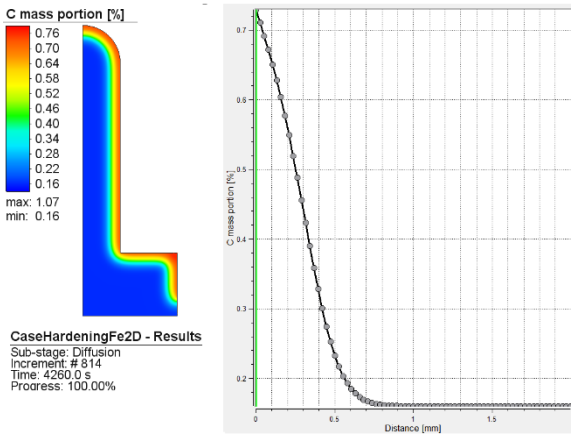

Figure 16: *Carbon profile at the end of stage Diffusion*

References

1. [Maximov, 2023] Maximov J., Duncheva G., Anchev A., Dunchev V., Anastasov K., Daskalova P., *Effect of Roller Burnishing and Slide Roller Burnishing on Surface Integrity of AISI 316 Steel: Theoretical and Experimental Comparative Analysis*, Machines 2024, 12, 51. https://doi.org/10.3390/machines12010051.
2. [Jászfi, 2022] Jászfi V., Prevedel P., Raninger P., Todt J., Mevec D., Godai Y., Maawad E., Ebner R., *Residual stress distribution of a locally and inductively quenched and tempered 50CrMo4 steel analysed by synchrotron transmission techniques*, Journal of Materials & Design 221 (2022) 110936.
3. [Holmberg, 2024] Holmberg J., Wendel J., Stormvinter A., *Progressive Induction Hardening: Measurement and Alteration of Residual Stresses*, *Journal of Materials Engineering and Performances* 33, 7770–7780 (2024), https://doi.org/10.1007/s11665-024-09703-0.
4. [Smirnov, 2023] Smirnov V., Lobanov D., Skeeba V., Golyushov I., *Improving the effi ciency of metal-bonded diamond abrasive end tools by improving manufacturing technology*, Metal Working and Material Science. 2021 vol. 23 no. 2 pp. 66–80.
5. [Pinheiro, 2024] Pinheiro P.M.; Junio J.U., Gonçalves L.A.P., da Costa J.Â.P., Ochoa A.A.V., Alves K.G.B., Leite G.d.N.P., Michima P.S.A, *Modeling and Simulation of the Induction Hardening Process: Evaluation of Gear Deformations and Parameter Optimization Processes*, 12, 1428, https://doi.org/10.3390/pr12071428.
6. [Spezzapria, 2016] Spezzapria M., Forzan M., Dughiero F., *Numerical Simulation of Solid-Solid Phase Transformations During Induction Hardening Process*, IEEE Transactions On Magnetics, Volume 52Issue 3, 2016.
7. [Javaheri, 2019] Javaheri V., Asperheim J.I., Bjørnar G., Nyo T.T., Porter D., *Simulation and experimental studies of induction hardening behavior of a new medium-carbon, low-alloy wear resistance steel*, International Symposium

on Heating by Electromagnetic Sources (HSE-19), May 22-24 (2019), Padova, Italy.

8. [Mühl, 2020] Mühl F., Damon J., Dietrich S., Schulze V., *Simulation of induction hardening: Simulative sensitivity analysis with respect to material parameters and the surface layer state*, Computational Materials Science, Volume 184, 2020.
9. [Perez-Santiago, 2024] Perez-Santiago, R., Hendrichs N.J., Capilla-González G., Vázquez-Lepe E., Cuan-Urquizo E., *The Influence of the Strain-Hardening Model in the Axial Force Prediction of Single Point Incremental Forming*, Appl. Sci. 2024, 14, 5705,

https:// doi.org/10.3390/app14135705,

10. [***, 2019] ***, *Simufact Forming Theory* manual. Computational Applications and System Integration Inc., 2019.
11. [Basliu, 2016] Basliu V., Vlad M., Movileanu G., *Composites with technological role by embedding granular particles of FeTi30 into a metallic matrix*, Journal of Science and Arts Year 2016, No. 4(37), pp. 385-394, 2016 ISSN: 1844 – 9581.
12. [Basliu, 2017] Basliu V., Vlad M., Movileanu G., *Obtaining composite materials with technological role by incorporating granular particles in metal matrix*, Advanced Materials Research, ISSN: 1662-8985, Vol. 1143, pp 79-84, doi:10.4028/www.scientific.net /AMR. 1143.79, © 2017 Trans Tech Publications, Switzerland.
13. [Basliu, 2011] Basliu V., Potecașu F., *Research Regarding the Obtaining of Some Composite Materials with Metallic Matrix from Aluminium and FeTi (32% Ti) Refractory Particles*, The Annals of "Dunarea de Jos" University of Galati. Fascicle IX, Metallurgy and Materials Science, vol. 34, no. 1, pp. 57-60, Mar. 2011.